Recurrence in plasma edge turbulence

M. S. Baptista,[a] I. L. Caldas, M. V. A. P. Heller, and A. A. Ferreira
Instituto de Física, Universidade de São Paulo, C. P. 66318, CEP 05315-970 São Paulo, S.P., Brazil

R. D. Bengtson
Fusion Research Center, The University of Texas at Austin, Austin, Texas 78712

J. Stöckel
Institute of Plasma Physics, Academy of Sciences of the Czech Republic, Za Slovankou 3. P.O.B. 17, 182 21 Praha 8, Czech Republic

(Received 7 May 2001; accepted 16 July 2001)

Common statistics of turbulent electrostatic fluctuations observed at the plasma edge and scrape-off layer are analyzed in three tokamak devices that have different configurations. The statistics of experimental data collected using fixed sampling time is the same than the statistics of the time for which the oscillation return to a specified reference interval of values. This observation, in addition to the finding of power-scaling laws for some average quantities with respect to either the sampling time or the size of the reference interval, suggests that turbulence on tokamaks have recurrent characteristics, typical of a recurrent chaotic low-dimensional system. Furthermore, the first Poincaré recurrence time and other dynamical tools are used to simulate the mentioned fluctuation statistical properties. © *2001 American Institute of Physics.* [DOI: 10.1063/1.1401117]

I. INTRODUCTION

The interest in plasma-edge turbulence in confinement devices is based on the evidence that improvements of plasma confinement depend on the plasma edge behavior.[1,2] Remarkably, experiments show that anomalous edge particle transport is induced by electrostatic turbulence.[3] Thus, it is important to identify the main characteristics of this turbulence and its dynamics.

Turbulent data, as obtained by plasma fluctuations, atmosphere fluctuations, flow velocity of oceanic streams, and others, have been extensively analyzed using low-dimensional tools.[4–12] However, the results are not always conclusive, and the main reason is that turbulent data reflects a dynamics dominated by structures of mixed dimension and different time scales, not comprised in those low-dimensional tools. Here, we propose another tool of analysis that measure the turbulent data in accordance with structures varying on space–time.

The main purpose of this work is to report new recurrent properties of tokamak turbulence and to use dynamical system theory to explain these statistical properties. We propose that a recurrent measure of chaotic dynamics, the first Poincaré return time,[13] is the proper tool to simulate such statistical observations. So, recurrent chaotic measurements[14,15] lead us to describe the observed turbulence recurrence as the result of dynamically recurrent cycles. As a consequence of these cycles, the statistics of experimental data collected using fixed sampling time is the same than the statistics of the time for which the oscillation return to a specified reference interval of values. This analysis is robust to data obtained from a system that presents mixed spatial dimension and structures with different time scales. Dynamical system theory is also applied to explain the existence of power-scaling laws for the average width of the distributions of the fluctuations observed on the data.

Here, we analyze the statistics of the fluctuating electrostatic measurements of three tokamaks, TEXTU (Texas University Tokamak),[16] CASTOR (Czech Academy of Sciences Torus),[17,18] and TBR (Brazilian Tokamak),[19,20] with different field configurations and plasma profiles and specific electrostatic turbulent behavior.

As the result of complex interaction of nonlinear processes,[21–24] electrostatic plasma edge fluctuations are believed to present statistics of both chaotic[11,12,25] and stochastic systems.[26] The former are deterministic, while the later are probabilistic, and only the former are sensible to initial conditions. Our description accounts for this once the first Poincaré return time, even though it can only be generated by a deterministic chaotic system, has properties of variables on the boundary between the chaotic deterministic behavior and the stochastic behavior. In fact, such chaotic measure can be used as a way to generate pseudorandom numbers.[27,28]

The outline of this paper is as follows: Sec. II gives a brief description of the analyzed experimental data. In Sec. III, we describe a few statistical properties of the experimental data, which we show to be typical of a low-dimensional system presented in Sec. IV to construct a statistical model for the fluctuations observed in the TEXTU tokamak. The application of this model for the other tokamaks is shown in Sec. V. In Sec. VI we summarize the conclusions of this work.

[a]Electronic mail: murilo@if.usp.br

II. EXPERIMENTAL DATA

Initially, we summarize the fundamental characteristics of electrostatic turbulence observed in three tokamak devices that have different configurations: TEXTU,[16] CASTOR,[17,18] and TBR.[19,20]

In TEXTU, the main parameters were major radius $R_0 = 1.05\,\mathrm{m}$, minor radius $a = 0.27\,\mathrm{m}$, toroidal magnetic field $B_t = 2.0\,\mathrm{T}$, plasma current $I_p = 200\,\mathrm{kA}$, chord averaged density $n_0 = 2.5 \times 10^{19}\,\mathrm{m}^{-3}$, pulse length of 100 ms, and safety factor at the limiter $q(a) \approx 3.5$. Data were collected by a probe positioned at the top of the vessel that measures floating potential fluctuations, V, at the radial position $r/a = 1.01$.[16] Signals were sampled at a rate of 2 MHz, for simulations we choose a time series of 75 ms.[16]

In CASTOR tokamak, data were collected in the scrape-off layer by two arrays of Langmuir probes (ten tips spaced poloidally by $d = 0.005\,\mathrm{m}$), which were spaced toroidally by 0.010 m.[17,18] The first array measured the ion saturation current and the second one measured the floating potential. The main plasma parameters in this experiment were major radius $R_0 = 0.40\,\mathrm{m}$, minor radius $a = 0.085\,\mathrm{m}$, toroidal magnetic field $B_t = 1.0\,\mathrm{T}$, plasma current $I_p = 6.0\,\mathrm{kA}$, pulse length of 25 ms, and safety factor at the limiter $q(a) \approx 15$. We choose for the analysis the floating potential from the probes located in the equatorial plane measured at $r/a = 1.06$. Signals were sampled at a rate of 308 kHz. Calculations were done on samples after high-pass digital filtering with a cutoff frequency of 1.5 kHz.

In TBR, data were collected at plasma edge and in the scrape-off layer from a multipin Langmuir probe.[19] This multipin tungsten probe was composed by four tips, a four pin probe array, and a single probe tip. The main plasma parameters in this experiment are major radius $R_0 = 0.30\,\mathrm{m}$, minor radius $a = 0.08\,\mathrm{m}$, toroidal magnetic field $B_t = 0.4\,\mathrm{T}$, plasma current $I_p = 10\,\mathrm{kA}$, chord average density $n_0 = 1 \times 10^{19}\,\mathrm{m}^{-}3$, pulse length of $\approx 8\,\mathrm{ms}$, and safety factor $q(a) = 4.5$. The considered floating potential fluctuations were measured at $r/a = 0.85$. The data sampling frequency was 1 MHz, time series measurements of approximately 4 ms were averaged and recorded over seven consecutive shots. The present analysis consider the fluctuations with or without external resonant magnetic field perturbation. The magnetic field perturbation was created by $m/n = 4/1$ electric current circulating in a set of resonant helical windings (RHW) located externally around the torus. The current circulating in those windings was adjusted at $I_h = 280\,\mathrm{A}$,[19,20] and it was switched on after the plasma current has reached steady values. The resonant magnetic perturbation changes remarkably the equilibrium parameters and fluctuating quantities at the plasma edge.

III. ANALYSIS OF TURBULENCE

Generally, for turbulence measurements, the space where such dynamics is reconstructed[29–31] is higher dimensional. Such space is called embedding space and its dimension, D_e, must respect the formula by Takens,[29] $D_e \geqslant 2D_0 + 1$, where D_0 is the fractal dimension of the data.

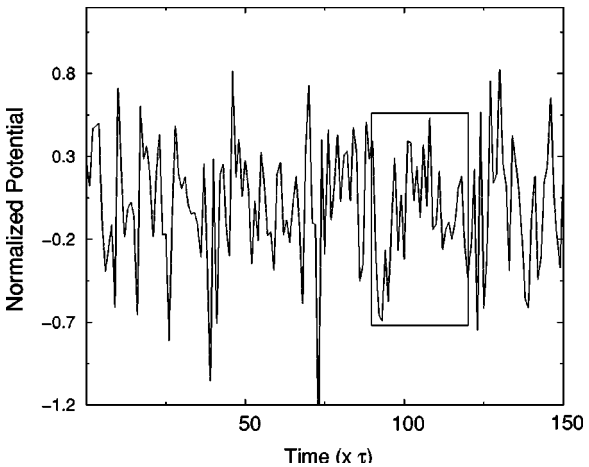

FIG. 1. Sample of the normalized fluctuating plasma potential, $eV(t)/kT_e$, in the tokamak TEXTU. Sampling rate $\tau = 0.5\,\mu\mathrm{s}$.

Reconstructing the dynamics even for higher-dimensional systems can be (after some effort) achieved. However, we cannot say the same for hard turbulent systems, where such reconstruction tools have given no convincing results, as for weather evolution data,[4] where a large series of papers have dealt with this subject. We argue that previous dynamical tools are not efficient to describe the dynamics of hard turbulent systems, because it presents structures with different dimensions and different spatial scalings. However, previous tools may be useful to describe soft turbulence with low dimension variability.[32,33] In fact, convection is a process of flows which can be well described by tools of low-dimensional systems.

A consequence of having a system with different dimensions is that its evolution cannot be well described by the trajectory, but only by statistical measurements. Consequently, a statistical analysis based on a scalar dynamical tool would be appropriate to describe turbulence. Such tool is the Poincaré first return time, which measures the time a chaotic trajectory takes to return to some interval of size ϵ in the phase space.[13]

There are two basic measurements, represented by M_t and M_s, to collect data from an experiment. We either set a sampling time and then measure some quantity using that time interval window (M_t), or we set some state we want to observe, and then, measure the time the system takes to return to that state (M_s). The first kind of measurement is usually the one used to make measurements. The second kind is frequently used when there is no way to make measurements of the first kind, as is the case for the spikes in neurons,[34] the time interval between drops in the dropping faucet experiments,[35] and heart beats.[36] These procedures can be applied to the tokamak measurements, by analyzing the statistical properties of either M_t or M_s.

In order to explore these dynamical interpretations of the turbulent fluctuations, we initially analyze data from the TEXTU to characterize the recurrent statistic of turbulence in the scrape-off layer. Figure 1 shows a sample of the normalized plasma potential fluctuations, $eV(t)/kT_e$, considered in this work. In Fig. 2 we see a magnification of Fig. 1, with

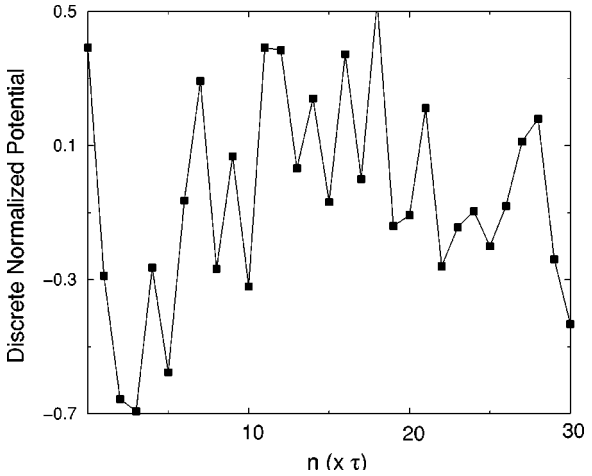

FIG. 2. Magnification of the box in Fig. 1, showing the values $V_n = eV(n\tau)/kT_e$. Sampling rate $\tau = 0.5\,\mu$s.

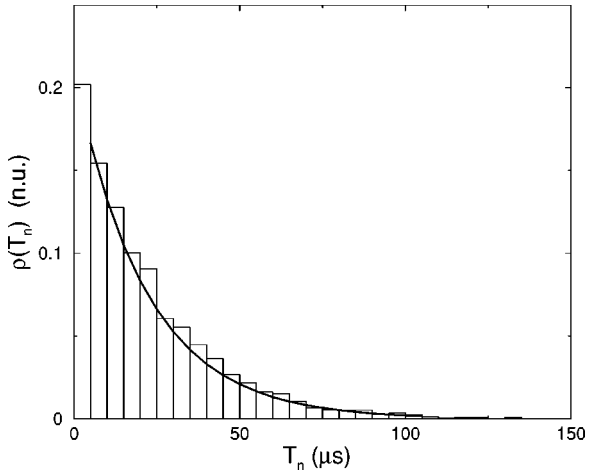

FIG. 4. Distribution of the return time of the fluctuations, for the experimental data shown in Figs. 1 and 2.

squares representing the values $V_n = eV(n\tau)/kT_e$. In this figure $\tau = 0.5\,\mu$s, where τ is the sampling rate, much lower than the autocorrelation time of this data that is approximately $9\,\mu$s.[16]

Initially we analyze a measurement of type M_s. For this, we measure the time, T_n, for which V_n reaches a reference interval $I = [-\epsilon, \epsilon]$, with $\epsilon = 0.016$. In Fig. 3 we show a schematic representation on how we measure the series of T_n. The value of ϵ is chosen such that is considerably bigger than the experiment precision and small enough to have many different values of return times, i.e., T_n must have significant statistics. Within this interval, the results are not sensible to changes in ϵ.

We first note that the probability distribution of T_n, $\rho(T_n)$, which can be seen in Fig. 4, is a Poisson distribution given by

$$\rho[T_n] = \mu e^{-\mu T_n} \tag{1}$$

with $\mu = 0.0116 \pm 0.0003\ (\mu s)^{-1}$ (obtained by the fitting), $\langle T_n \rangle = 21.8\,\mu$s, the average value of all T_n's, obtained by the data (as expected $\mu = 1/\langle T_n \rangle$).

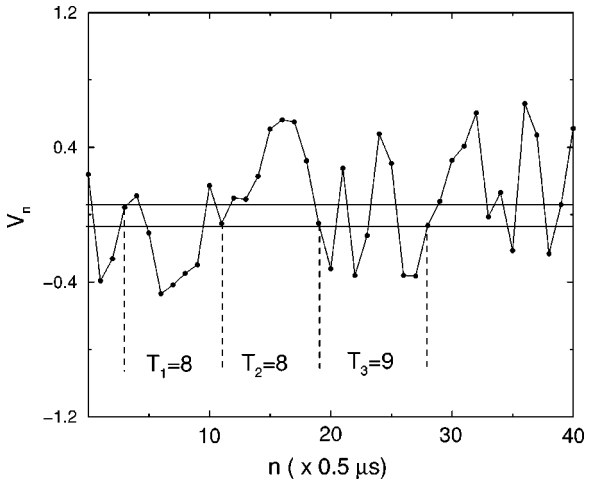

FIG. 3. Sample of the data of Fig. 1 and the representation of the three return time T_n are indicated for an out-of-scale half-interval ϵ.

Another verification about the data is that there is a scaling-power law relating the average value $\langle T_n \rangle$ with the reference interval half width ϵ, given by

$$\langle T_n \rangle \propto \epsilon^{-\alpha} \tag{2}$$

with $\alpha = 0.943 \pm 0.016$.

The analyzed data present characteristics of both deterministic and stochastic processes.

Among the deterministic characteristics we mention the fact that there are a few limitations on the sequence of values for T_{n+1}, depending on T_n, indicating that T_n is not completely stochastic. Also, the values of T_n are restricted to a finite interval. Moreover, if we construct a set W_n, with elements representing the sum of q subsequent elements of T_n, i.e., $W_1 = T_1 + T_2 + \cdots + T_q$, $W_2 = T_{q+1} + T_{q+2} + \cdots + T_{2q}$, and so on, we noticed that

$$\langle W_i(q) \rangle = q \langle T_n \rangle. \tag{3}$$

As far as the stochastic characteristics we cite that the linear correlation between T_{n+1} and T_n is close to zero, a property of stochastic data.

Once fluctuating measurements are often oscillating around a time-varying offset, it is often appropriate to work with a new variable, A_n, defined to be

$$A_n = T_{n+1} - T_n. \tag{4}$$

Such variable difference has the advantage of not changing any one of the statistical properties described previously, and also, A_n oscillates around zero, avoiding tendencies on T_n.

Next, to analyze a measurement of type M_t, we examine another oscillation difference, denoted by R_n and given by

$$R_n = V_{n+1} - V_n. \tag{5}$$

For the series R_n we obtain the probability distribution $\rho(R_n)$ shown in Fig. 5. This probability distribution can be represented as

$$\rho(R_n) = \sigma \exp -(|R_n - \langle R_n \rangle| / \langle R_n^+ \rangle), \tag{6}$$

which corresponds to a sum of two Poisson distributions. σ is proportional to $1/\langle R_n^+ \rangle$, $\langle R_n \rangle$ is the average of the R_n's,

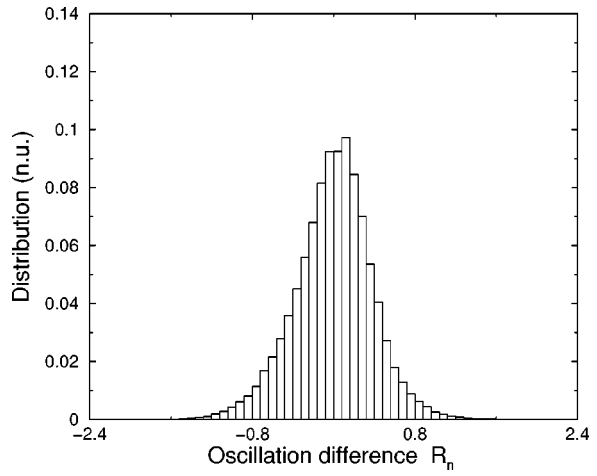

FIG. 5. Distribution of the oscillation differences, $R_n = V_{n+1} - V_n$, of the TEXTU experimental data.

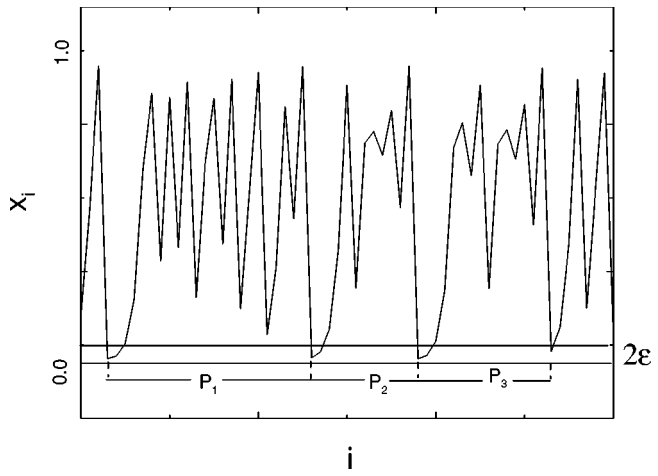

FIG. 7. Chaotic orbit for Eq. (8). The first three Poincaré return times are indicated for an out-of-scale half-interval of size ϵ.

and R_n^+ is a R_n bigger than $\langle R_n \rangle$. This Poisson-type distribution is characterized by the average width of the distribution, which is equal to $\langle R_n^+ \rangle$.

We can identify a scaling law relating the distribution of the oscillation difference calculated for a time interval $M\tau$, shown in Fig. 6,

$$\log[\langle R_n^+(M\tau)\rangle] \propto M^{0.45}. \tag{7}$$

The power-law relation indicates a growth of the width with M. In the limit of a high value of M the Poisson-type distribution becomes a Gaussian one. The central limit theorem predicts such limit for stochastic variables. Thus, this transition to the Gaussian distribution suggests that R_n would behave as a stochastic variable for high M. On the other hand, for extremely small M, all the data are correlated. Therefore, observation of the system for a nonappropriate sampling rate can hide its dynamical properties.

Statistics of the return time of the fluctuations to a given specified interval of values [Eqs. (1) and (2)] might reflect the metric characteristics of the trajectory of a dynamical system in the phase space. On the other hand, the same kind of statistics [Eq. (6)] is also obtained by other measures involving relative fluctuations in a fixed time. Thus, the return time is a measurement of type M_s for a specified position in phase space, while the relative fluctuation is a measurement of type M_t for a fixed sampling time. We suggest that both kinds of statistics reflects the same metric characteristics as it is the case in ergodic dynamical systems.

We summarize this section by saying that the edge turbulence has the following properties: (a) the fluctuation distribution is an invariant measure along the time; (b) the statistics of both variables, A_n and R_n, are described by Poisson-type distributions, what suggests that these variables are recurrent.

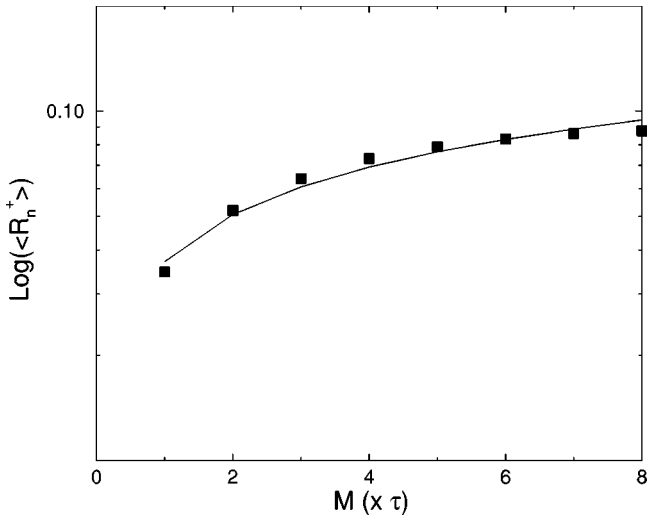

FIG. 6. Scaling power-law for $\langle R_n^+ \rangle$ (squares) with respect to the measuring sampling rate, $M\tau$, with $\tau = 0.5\,\mu$s. The line represents a fitted curve.

IV. STATISTICAL MODELING

The observed turbulent fluctuations presents statistics that can be found in low-dimensional chaotic systems. These properties are due to a common recurrent property present in these systems. This section is dedicated to show how these observed statistical properties emerge from measures of the Logistic map,

$$x_{i+1} = c x_i (1 - x_i), \tag{8}$$

with the control parameter $c = 4.0$.[37] The recurrence is introduced through a sequence of values P_n, the first Poincaré return time of the chaotic orbit, i.e., the number of map iterations required for the orbit to reach twice a specified small interval $J = [0.100, 0.100 + \epsilon]$.[13,15] To illustrate the return time calculation, Fig. 7 shows the chosen chaotic evolution x_i and three successive values of P_n.

Furthermore, Fig. 8 shows the distribution of the first Poincaré return time calculated according this procedure, for $\epsilon = 0.005$. The density distribution $\rho(P_n)$ can be theoretically obtained[13]

$$\rho[P_n(\epsilon)] = \beta e^{-P_n(\epsilon)/\langle P_n(\epsilon)\rangle}, \tag{9}$$

where β can be scaled to $1/\langle P_n \rangle$, such that (9) is a probability distribution. $\langle P_n \rangle$ is the average value of the series of P_n's.

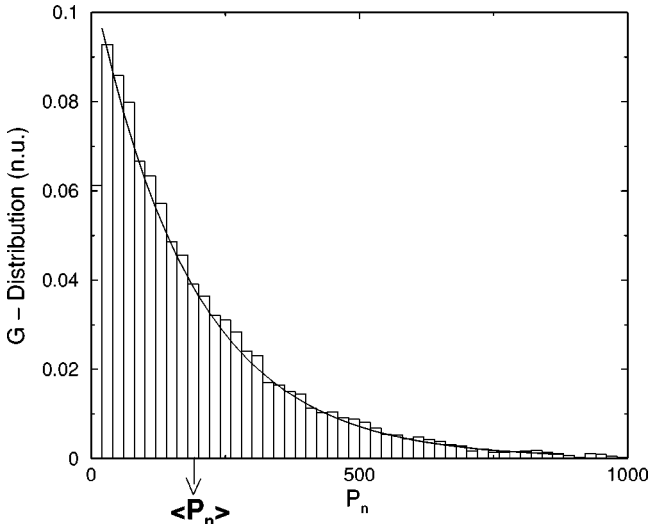

FIG. 8. Distribution of the first Poincaré return time, P_n, for a specified reference interval.

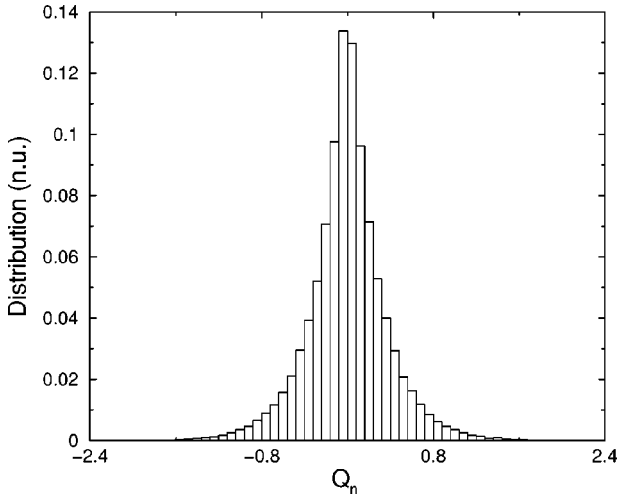

FIG. 9. Distribution of Q_n that simulates the experimental distribution shown in Fig. 5.

The Poincaré first return time, although calculated from the chaotic trajectory, measures the periods of the infinitely many unstable periodic orbits embedded in the chaotic attractor.[13] In other words, the Poincaré time measures how recurrent is the dynamical system.

By proposing the description of a measure of the considered plasma fluctuations by the use of this Poincaré time, we are taking into account the periodic cycles that might exist in the turbulent plasma. However, the distribution $\rho(P_n)$ is not the same type of the distribution $\rho(R_n)$. So, it is convenient to work with a new variable Q_n which is the subtraction of two dynamically generated series,

$$Q_n(\epsilon)=P_n(\epsilon,x_0)-P_n(\epsilon,x_0'). \tag{10}$$

The convolution of $\rho[P_n(\epsilon,x_0)]$ with $\rho[P_n(\epsilon,x_0')]$ is equal to $\rho[Q_n(\epsilon)]$. Note that $\rho(Q_n)$ does not depend on neither x_0 nor x_0', and that is a consequence of the fact that Eq. (8) has an ergodic trajectory, and thus, $\rho[P_n(\epsilon,x_0)]=\rho[P_n(\epsilon,x_0')]$. We find that

$$\rho(Q_n)=\frac{\beta}{2}e^{\beta Q_n}, \tag{11}$$

where $\beta=1/\langle P_n\rangle$, which means that the slope of this probability distribution is determined by $\langle P_n\rangle$.

In fact, the scaling of $\langle P_n\rangle$ with ϵ does not only tell us about the width of its distribution, but it tells us about the fractal dimension[38] of the dynamical system involved. So, numerically, we find that

$$\langle P_n(\epsilon)\rangle\propto\epsilon^{-\sigma}, \tag{12}$$

where $\sigma=0.994\pm0.005$. By[13] the average value $\langle P_n\rangle \propto\epsilon^{-p/D_0}$, where D_0 is the fractal dimension, which should be close to one for Eq. (8), and p is the Pesin dimension which for this case is also close to one, once $p/D_0=0.994$.

Like observed experimentally in turbulent fluctuations, the series of P_n is not completely stochastic. This is due to dynamical constraints, that is, a few limitations on the possible values for P_{n+1}, depending on P_n. Also, if we construct a set W_i, with elements representing the sum of q subsequent elements of P_n, i.e., $W_1=P_1+P_2+\cdots+P_q$, $W_2=P_{q+1}+P_{q+2}+\cdots+P_{2q}$, and so on, we noticed that

$$\langle W_i(q)\rangle=q\langle P_n\rangle. \tag{13}$$

Equation (13) is a consequence of the fact that average quantities of the series of P_n is invariant to the initial condition, a consequence of ergodicity.

In order to understand the relation between the fluctuating amplitude measured in the experiment (proportional to the period of the cycles present in the turbulent electrostatic fluctuations) with the average period of the cycles in Eq. (8) (which is proportional to the length of the interval J), we just have to compare Eq. (7) with Eq. (12). In other words, we can relate the amplitude of the turbulent oscillations with the size of the interval J, introduced to obtain P_n.

The turbulent fluctuation distribution of Sec. III can be simulated by introducing a series Z_n such that

$$Z_{n+1}=Z_n+Q_n, \tag{14}$$

where we rescale Q_n by using the property $\rho[P_n(x_0')]=\rho[P_{n+1}(x_0)]$,

$$Q_n=(aP_n-bP_{n+1})/F, \tag{15}$$

where

$$F(\tau,\epsilon)=\frac{\langle P_n(\epsilon)\rangle}{\langle R_n^+(\tau)\rangle}, \tag{16}$$

$$b(\tau,\epsilon)=\frac{F\langle R_n^-(\tau)\rangle\langle R_n^+(\epsilon)\rangle}{\langle P_n(\epsilon)\rangle[\langle R_n^-(\tau)\rangle-\langle R_n(\tau)\rangle]}, \tag{17}$$

and

$$a=b\left[1.0-\frac{\langle R_n(\tau)\rangle}{\langle R_n^-(\tau)\rangle}\right]=1.0. \tag{18}$$

Using Eqs. (16) and (17) with $\langle R_n\rangle$, R_n^+, and R_n^- calculated using the data of Fig. 1, we generate the series of Z_n.

Figure 9 shows the distribution of the simulated data Q_n [obtained by using Eq. (15)], reproducing quite well the ex-

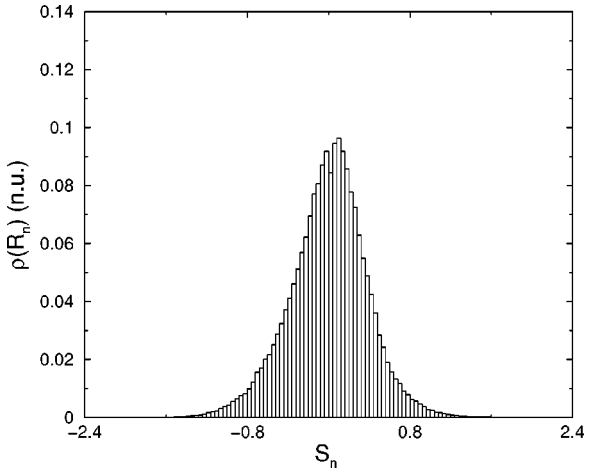

FIG. 10. Distribution of the simulated $S_n = Y_{n+1} - Y_n$.

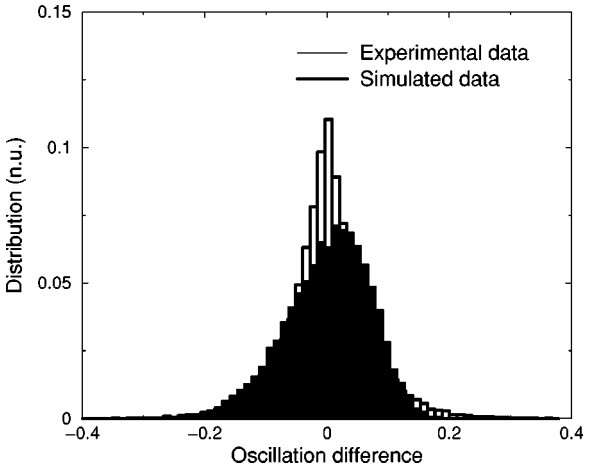

FIG. 11. Distribution of the oscillation differences R_n for the Castor Tokamak and the distribution of the simulated Q_n.

perimental distribution (Fig. 5). In this case we use $F = 683.880$ and $b = 1.000$, calculated by Eqs. (16) and (17), using $\langle R_n \rangle = -4.306 \times 10^{-6}$, $R_n^+ = 0.272$, and $R_n^- = -0.296$ from the data of Fig. 1 ($\langle Q_n \rangle = -2.099 \times 10^{-6}$, $Q_n^+ = 0.264$, and $Q_n^- = -0.264$).

Instead of using the first Poincaré return time to simulate the distribution of Fig. 5, we can obtain this distribution by using a measurement of type M_s of the chaotic system. Inspired by our previous considerations, according to which the oscillation difference should present geometric characteristics of turbulence, we choose a measurable of chaotic system closely related to the fractal dimension; the minimum average distance of a set of trajectories in a region of the phase space.

So, to reproduce the results from Fig. 5 (for the TEXTU turbulence) we do the following. We get a collection of 5000 initial conditions of the logistic map, equally spread over the interval [0,1], and iterate them using Eq. (8). After a few iterations, we measure the average minimum distance, Y_n, between pair of points that fall within the interval $J = [0.8 - \epsilon, 0.8 + \epsilon]$ (with $\epsilon = 0.05$). Thus, we define the relative variable, S_n, in the same way of Eq. (5),

$$S_n = Y_{n+1} - Y_n \tag{19}$$

whose distribution $\rho(S_n)$, shown in Fig. 10, is of the same type of the distribution of Fig. 5.

Also, a scaling-power law can be obtained relating $\langle S_n \rangle$, with S_n calculated by Eq. (19), with the half-interval ϵ, $\langle S_n \rangle \propto \epsilon^{1/D_0}$, where D_0 is the fractal dimension of the attractor of Eq. (8).

So, the theoretical P_n is equivalent to the experimental T_n and S_n is equivalent to R_n. In addition, both P_n (and T_n) or S_n (and R_n) reflect the same metric of the system.

Let us explain the scaling-power law of Fig. 6, which scales up to $M = 10$, and then breaks the scale. We mention the fact that there exist a very short-range correlation of the series of R_n given by Eq. (5). Consequently, it is often common to set the sampling rate to be much lower than the time for the correlation to decay $1/e$. Such behavior could be well simulated by either Eq. (15) or Eq. (19) if we impose a constrain on the ''creation'' of values P_n or T_n. For example, we could impose that P_{n+1} should fall within the interval $[P_n - k, P_n + k]$, where k is proportional to the time for the correlation to decay to zero.

On the remaining of the paper, all the simulations will use the variable of Eq. (15) to simulate Eq. (5). This is due to the fact that both variables, the one given by (19) and the one given by Eq. (15), should contain the same type of information.

In conclusion, statistical measures of the analyzed turbulent data (properties a and b at the end of Sec. III) are also observed in a low-dimensional system. This suggests that the experimental variables may be described in terms of the first Poincaré return time of low-dimensional chaotic systems.

V. OTHER APPLICATIONS

In this section we apply the dynamical description introduced in this work to analyze the recurrent statistics observed in the electrostatic fluctuations under other conditions of turbulence, in the tokamaks CASTOR and TBR, described in Sec. II.

Using a sample of plasma potential fluctuation measured at the scrape-off layer in the tokamak CASTOR,[17,18] we calculate the experimental distribution of the relative fluctuation, R_n, shown in Fig. 11. This distribution can be simulated by the distribution of the Q_n values, obtained by a linear combination of two first Poincaré return time calculated for the chaotic trajectory in Eq. (8). In this case we use $F = 145.789$, calculated by Eqs. (16), with $\langle R_n \rangle = 4 \times 10^{-6}$, $R_n^+ = 0.052$, and $R_n^- = -0.061$, calculated from the experimental data.

We repeat this procedure to compare the electrostatic fluctuation distribution observed in the tokamak TBR.[19,20] In this case the turbulent fluctuations were measured at the plasma edge with and without external resonant magnetic perturbations created by helical windings.

The data are presented in Figs. 12(A) (without helical windings) and 12(B) (with helical windings). We see that the high peaks of amplitudes are eliminated by introducing the external resonant magnetic field. Consequently, the remained

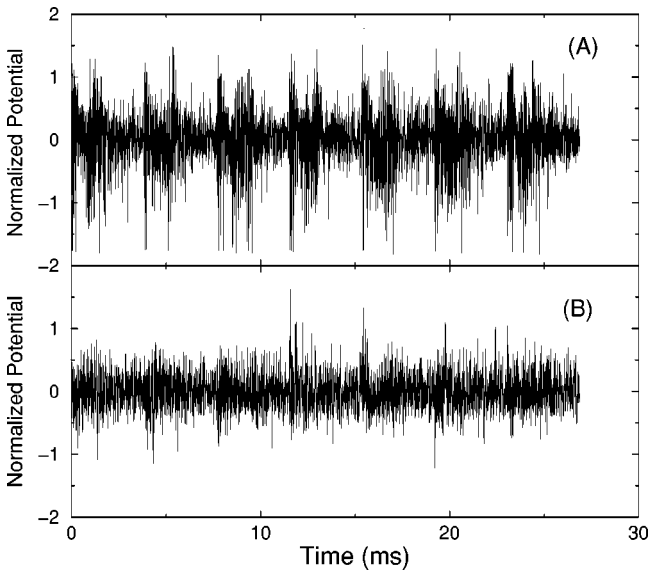

FIG. 12. The normalized fluctuating plasma potential, eV/kT_e, in the tokamak TBR without (A) and with (B) resonant helical windings. Sampling rate $\tau=1\ \mu$s.

power is spread over a broader frequency region in the spectrum, what indicates a higher turbulent fluctuation.

Figure 13 shows the experimental ($\langle R_n\rangle=2.148\times10^{-4}$, $R_n^+=0.057$, $R_n^-=-0.055$) and the simulated distributions for the spontaneous turbulence ($\langle Q_n\rangle=2.220\times10^{-4}$, $Q_n^+=0.054$, $Q_n^-=-0.053$, $F=133.010$, and $b=0.996$), whereas Fig. 14 ($\langle R_n\rangle=8.592\times10^{-5}$, $R_n^+=0.101$, $R_n^-=-0.096$, $\langle Q_n\rangle=8.950\times10^{-5}$, $Q_n^+=0.095$, $Q_n^-=-0.094$, $F=377.514$, and $b=0.999$) shows the same for the turbulence perturbed by the resonant helical windings. Comparing these figures, we see that the perturbation of helical windings that enhances the turbulence increases the distribution width. This can be described by calculating the exponent α of Eq. (2), which increases with the width. For the data of Fig. 12(A), $\alpha=0.959\pm0.049$, and for the data of

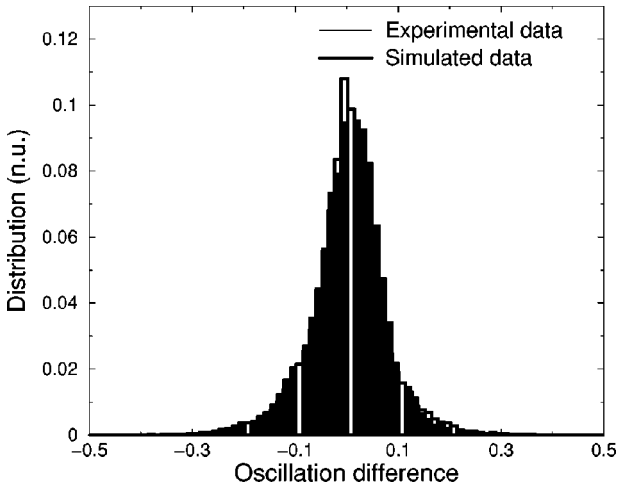

FIG. 13. Distribution of the oscillation differences R_n for data of the TBR Tokamak without resonant helical windings, and the distribution of the simulated Q_n.

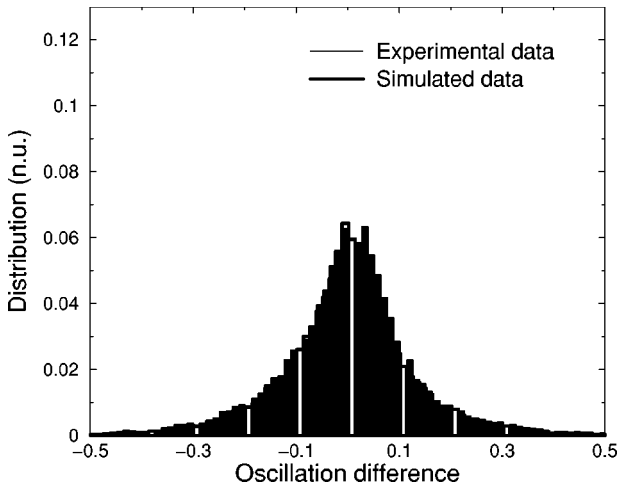

FIG. 14. Distribution of the oscillation differences R_n for data of the TBR Tokamak with resonant helical windings and the distribution of the simulated Q_n.

Fig. 12(B), $\alpha=0.968\pm0.009$, indicating that the plasma with helical windings is more turbulent.

To characterize how turbulent are the data, we suggest that the average time of the recurrent cycles measures the property of mixing. In fact, mixing is a property related to the ability a dynamical system has to spread a set of initial conditions in different portions of the phase space. So, for a higher mixing system, the average return time of one variable is lower and, therefore, the exponent α, obtained from the data, and σ, obtained from the simulation [Eq. (12)], are higher.

Modeling the recurrence of a turbulent system by the recurrence of a chaotic system requires that $\alpha\leqslant\sigma$, because if $\alpha>\sigma$, the data has dynamics not reproduced by the modeling dynamical equation. In particular, the exponent σ of Eq. (12) is higher for higher mixing (more chaotic) systems, what can be accomplished by increasing the control parameter c. Note that $c\leqslant4$, so the maximum value of σ for Eq. (8) is $\sigma=0.994\pm0.005$, for $c=4$ (as used in this work). Thus, as α approaches 1, the data recurrence tends to present more stochastic characteristics.

The highest exponent $\alpha=0.983\pm0.007$, is from the Castor tokamak. This high exponent suggests that the recurrence observed in this tokamak might have stochastic components. This might be the reason for the Gaussian-type shape on the right-hand side of the distribution of Fig. 11, indicating that stochastic-like behavior is already substantial in the recurrence of that data.

Note that the parameter α does not depend on the fluctuation normalization. Usually, the ratio $e\langle V_n\rangle/k\langle T_e\rangle$ (which is proportional to $\langle R_n\rangle$) is used to differentiate strong from weak turbulence. Here, instead of the average fluctuation amplitude, we suggest the mixing associated to the measures to have an estimation of how turbulent the system is, i.e., more turbulent the system is, less time the measurement takes to return to a given reference interval, following Eq. (2).

We suggest that evidences of strong or weak turbulence might be given whether α is higher or lower, respectively.

VI. CONCLUSION

It is commonly accepted that turbulence presents behavior typical of complex systems.[14,15,26,39,40] These systems are believed to have among other structures its own self-organized structures,[14] as well as, the existence of many infinitely periodic cycles. The analysis done here and the derivation of the proposed statistical modeling takes advantages of the existence of such cycles in turbulent systems. Despite all the complexity involved in turbulent data, once such cycles exist, simple low dimensional chaotic dynamical systems can well describe the statistical manifestations of this cyclic turbulence.

The proposed statistical analysis of this paper, introducing a simple way of observing turbulence, by registering its recurrent cycles, has also been done in other considered complex systems, as the New York Stock Market index oscillations,[41] the changing of the maximum temperature of the San Francisco Bay area, and the appearance of the amino acids, in the DNA sequence of the *M. Genitalium* bacteria.[42]

The finding of a Poisson distribution for the return time (for fixed reference interval in the observable variables) and for the oscillation differences (for fixed sampling time) is due to the equivalence of these two measures, which reflect local metric characteristics of the hidden dynamical behavior result of the existence of recurrent cycles in these turbulent data.

We note three evidences of ergodicity in the analyzed plasma edge turbulence: (1) data are recurrent on return time and on the oscillation differences; (2) equivalence between analysis of return time and oscillation difference; (3) collection of measurements in different discharges is statistically equivalent to measurements in any single discharge, i.e., statistical analysis of a sample of a set is equivalent to the whole set.

All these described empirical properties can be appropriately simulated through the first Poincaré return time, and other tools that measures the recurrence in low-dimensional chaotic systems (as the logistic map used in this work).

Moreover, recurrence is a way to determine geometrical characteristics in low-dimensional dynamical systems. In analogy to this, we propose recurrence as a way to determine geometrical characteristics of turbulent data. Thus, while the parameter σ [Eq. (12)], that characterizes recurrence in a low-dimensional dynamical system, is proportional to the fractal dimension, α (2) obtained from the turbulent data should be a characteristic related to how much mixing is present in the data. In specific, smaller α corresponds to data with less mixing.

Finally, prediction for occurrence of events in turbulent and complex systems can be done with low-dimensional dynamical systems, which reproduce dynamical structures typical of those complex and turbulent systems, in specific, its recurrence. Thus, we do not propose a model for turbulence but rather a model for its recurrence.

ACKNOWLEDGMENTS

This work was partially supported by Brazilian governmental agencies FAPESP, CNPq, and CAPES.

[1] J. Wootton, B. A. Carreras, H. Matsumoto, K. McGuire, W. A. Peebles, Ch. P. Ritz, P. W. Terry, and S. J. Zweben, Phys. Fluids **2**, 2879 (1990).
[2] F. Wagner and V. Stroh, Plasma Phys. Controlled Fusion **35**, 1321 (1993).
[3] R. D. Hazeltine and J. D. Meiss, *Plasma Confinement* (Addison–Wesley, Redwood City, 1992).
[4] E. N. Lorenz, Nature (London) **353**, 241 (1991).
[5] L. P. Kadanoff, *From Order to Chaos* (World Scientific, New York, 1993).
[6] P. Holmes, J. L. Lumley, and G. Berkooz, *Turbulence, Coherent Structures, Dynamical Systems, and Symmetry* (Cambridge, New York, 1996).
[7] P. Civitanovik, *Universality in Chaos* (Adam Hilger, New York, 1989).
[8] U. Frish, *Turbulence: The Legacy of A. N. Kolmogorov* (Cambridge, New York, 1995).
[9] E. A. Spiegel, Proc. R. Soc. London **413**, 87 (1987).
[10] D. Ruelle, Proc. R. Soc. London **413**, 5 (1987).
[11] G. Y. Antar, P. Devynck, X. Garbet, and S. C. Luckhardt, Phys. Plasmas **8**, 1612 (2001).
[12] S. J. Zweben, D. Manos, R. V. Budny *et al.*, J. Nucl. Mater. **147**, 250 (1987).
[13] V. Afraimovich, Chaos **7**, 12 (1997).
[14] G. M. Zaslavsky, M. Edelman, H. Weitzner *et al.*, Phys. Plasmas **7**, 3691 (2000).
[15] G. M. Zaslavsky and M. K. Tippet, Phys. Rev. Lett. **67**, 3251 (1991).
[16] A. V. Filippas, R. D. Bengston, X. G. Lee, M. Meier, Ch. P. Ritz, and E. J. Powers, Phys. Plasmas **2**, 839 (1995).
[17] J. Stöckel, I. Duran, V. Dhyani, M. Hron, K. Jakubka, L. Kryska, V. Svoboda, F. Zacek, J. Petrzilka, I. Nanobashvili, and S. Nanobashvili, in *Proceedings of the 1996 International Conference on Plasma Physics, Nagoya, 1996* (International Atomic Energy Agency, Vienna, 1996), Vol. I, p. 322.
[18] J. Stöckel, V. Dhyani, K. Jakubka, L. Kryska, F. Zacek, I. Duran, M. Horn, and J. Petrzilka, in *Proceedings of the 24th European Physical Society Conference on Controlled Fusion and Plasma Physics, Berchtesgaden, 1997* (European Physical Society, Petit Lancy, 1997), Vol. 21A, p. 625.
[19] R. M. Castro, M. V. A. P. Heller, I. L. Caldas, Z. A. Brasilio, R. P. da Silva, and I. C. Nascimento, Phys. Plasmas **3**, 971 (1996); **4**, 329 (1997).
[20] M. V. A. P. Heller, R. M. Castro, I. L. Caldas, Z. A. Brasilio, R. P. da Silva, and I. C. Nascimento, J. Phys. Soc. Jpn. **66**, 3453 (1997).
[21] D. Biskamp, *Nonlinear Magnetohydrodynamics* (Cambridge, New York, 1993).
[22] S. J. Camargo and H. Tasso, Phys. Fluids B **4**, 1199 (1992).
[23] P. W. Terry, Rev. Mod. Phys. **72**, 109 (2000).
[24] P. J. Morrison, Rev. Mod. Phys. **70**, 467 (1998).
[25] D. F. Düchs, A. Montvai, and C. Sack, Plasma Phys. Controlled Fusion **33**, 919 (1991).
[26] R. Balescu, Eur. J. Phys. **21**, 279 (2000).
[27] W. H. Press, S. A. Teukolsky, W. T. Vetterling, and B. P. Flannery, *Numerical Recipes in Fortran 77* (Cambridge, New York, 1992).
[28] J. A. Gonzalez and R. Pino, Physica A **276**, 425 (2000).
[29] F. Takens, ''Detecting strange attractors in turbulence,'' in *Dynamical Systems and Turbulence*, edited by D. Rand and L. S. Young (Springer, Berlin, 1981).
[30] C. Letellier, J. Maquet, H. Labro, L. Le Sceller, G. Gouesbet, F. Argoul, and A. Arnéodo, J. Phys. Chem. A **102**, 10 265 (1998).
[31] R. Castro and T. Sauer, Phys. Rev. E **59**, 2911 (1999).
[32] Ying-Cheng Lai and Celso Grebogi, Phys. Rev. Lett. **82**, 4803 (1999).
[33] Ying-Cheng Lai, Celso Grebogi, and Jürgen Kurths, Phys. Rev. E **59**, 2907 (1999).
[34] E. M. Izhikevich, Int. J. Bifurcation Chaos Appl. Sci. Eng. **10**, 1171 (2000).
[35] R. D. Pinto, W. M. Gonçalves, J. C. Sartorelli, I. L. Caldas, and M. S. Baptista, Phys. Rev. E **58**, 1 (1998).
[36] T. C. Chou, *Electrocardiology in Clinical Practice* (Saunders, Philadelphia, 1991).
[37] Parameter $b=4$ is chosen such that Eq. (8) is equivalent to a Bernoulli shift, and thus presents orbits that visit everywhere the phase space. In other words, if trajectories are associated to symbols, any symbolic sequence is permitted.
[38] K. T. Alligood, T. Sauer, and J. A. Yorke, *Chaos, An Introduction to Dynamical Systems* (Springer-Verlag, New York, 1997).
[39] W. Horton, Phys. Fluids **29**, 1491 (1986).
[40] W. Horton, Rev. Mod. Phys. **71**, 735 (1999).
[41] M. S. Baptista and I. L. Caldas, Physica A **284**, 348 (2000).
[42] M. S. Baptista, I. L. Caldas, M. S. Baptista, C. S. Baptista, A. A. Ferreira, and M. V. A. P. Heller, Physica A **287**, 91 (2000).